*International Journal of Minerals, Metallurgy and Materials*
*Volume 26, Number 3, March 2019, Page 309*
**https://doi.org/10.1007/s12613-019-1739-3**

# Feasibility of aluminum recovery and $MgAl_2O_4$ spinel synthesis from secondary aluminum dross

*Yong Zhang, Zhao-hui Guo, Zi-yu Han, Xi-yuan Xiao, and Chi Peng*

School of Metallurgy and Environment, Central South University, Changsha 410083, China
(Received: 12 June 2018; revised: 9 October 2018; accepted: 25 October 2018)

**Abstract:** The feasibility of aluminum recovery from secondary aluminum dross by extraction with NaOH solution and the subsequent synthesis of $MgAl_2O_4$ spinel by sintering the extracted slag were studied. The extraction percentage of soluble aluminum from the dross reached 80% at a temperature of 353 K, liquid-to-solid ratio of 12 $mL \cdot g^{-1}$, stirring speed of 300 $r \cdot min^{-1}$, and an extraction time of 15 min; the hydrolysis percentage of AlN reached 40% with an extraction time of 30 min. The activation energies of the soluble aluminum and AlN extracted from the dross were 7.15 and 8.98 $kJ \cdot mol^{-1}$, respectively, indicating that their kinetics were controlled by outer diffusion without a product layer. The extracted slag was sintered in the temperature range 1373–1773 K; $MgAl_2O_4$ spinel with a compressive strength as high as 69.4 MPa was produced in the sample sintered at 1673 K for 3 h. This value exceeds the threshold (40 MPa) prescribed by the National Standard for the Magnesia and Magnesia–alumina Refractory Bricks of China (GB/T 2275—2007). These results establish the effectiveness of aluminum recovery from secondary aluminum dross and subsequent $MgAl_2O_4$ spinel synthesis.

**Keywords:** secondary aluminum dross; reuse; extraction; sintering; magnesium aluminate spinel

## 1. Introduction

Aluminum dross is widely generated because of extensive development of the secondary aluminum industry. However, most secondary aluminum dross is deposited in landfills without any pre-disposal treatment [1]. The adverse effects of this material on the natural environment have attracted great attention in recent years [2]. Ammonia gas ($NH_3$), chloride, and soluble aluminum are generated when the dross is in a landfill, and these compounds cause serious environmental problems [3–4]. Secondary aluminum dross containing approximately 5wt%–20wt% Al and a large quantity of soluble salts is usually known as black dross, and that containing 5wt%–10wt% Al is known as salt cake [5]. Appropriately disposing of and, wherever possible, reusing secondary aluminum dross are important to minimize its environmental risks. In Europe, this waste is forbidden from being deposited into landfills because the soluble salts in the slag could potentially pollute surface and groundwater supplies [5].

Generally, the treatment of aluminum dross includes milling, shredding, and subsequent granulometric classification [6]. The buried aluminum metal can react with alkaline species to form the water-soluble product $[Al(OH)_4]^-(aq)$ [7]. Aluminum extraction is one of the more effective methods of managing aluminum dross. The recovery of aluminum helps reduce the amount of waste deposited into landfills [8]. After recovery, the residue slag can be used as a raw material for spinel production, minimizing reagent addition and cost [9–10]. Magnesium aluminate ($MgAl_2O_4$) spinel is widely used in commercial applications [11–12] and has numerous attractive properties, such as a high melting point (2408 K), reliable mechanical strength, substantial chemical stability, high thermal shock resistance, and a low thermal expansion coefficient [13–15]. It has been used in various applications, including optical windows for pressure vessels and bullet-proof vehicles, alternative materials to replace the conventional carbon anode material in aluminum electrolytic cells, humidity sensors, and refractory materials for cement rotary kilns and steel

Corresponding author: Zhao-hui Guo E-mail: zhguo@csu.edu.cn

ladles [14]. Although the general calcination temperature can be as high as 1873 K, the additional costs to be borne in generating $MgAl_2O_4$ spinel are also high [16–17]. Moreover, the literature contains few studies on the use of secondary aluminum dross as a potential resource for $MgAl_2O_4$ spinel synthesis.

The development of environment friendly techniques to recycle secondary aluminum dross is important. The objectives of the present study were as follows: (1) to optimize the conditions for the extraction of the soluble aluminum and for the hydrolysis of AlN from secondary aluminum dross, (2) to study the kinetics of extraction of the soluble aluminum and AlN from the dross; and (3) to synthesis $MgAl_2O_4$ spinel from the extracted slag.

## 2. Experimental

### 2.1. Materials

Secondary aluminum dross was procured from a secondary aluminum plant in Jiangxi province, China. Prior to the experiment, the dross was dried and ground. Approximately 92.40wt% of the dross particles were smaller than 41.84 μm, and the average particle size was 23.42 μm. The composition of the dross, including its content of Al, Mg, Si, and other main elements, is shown in Table 1. The mineral phases of the dross were Al, α-$Al_2O_3$, $MgAl_2O_4$, and AlN (Fig. 1). Salts, calcium-containing compounds, and silicon compounds were the remaining constituents of the dross.

**Table 1. Chemical composition of secondary aluminum dross**

wt%

| Al | Mg | Si | Ca | Fe | Na | Ti | Others |
|---|---|---|---|---|---|---|---|
| 39.61 | 6.39 | 7.26 | 3.47 | 1.20 | 1.03 | 1.61 | 39.43 |

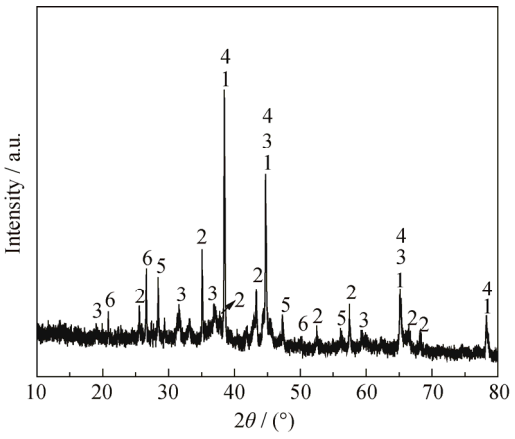


**Fig. 1. XRD pattern of secondary aluminum dross. 1—Al; 2—α-$Al_2O_3$; 3—$MgAl_2O_4$; 4—AlN; 5—ZnS; 6—$SiO_2$.**

### 2.2. Methods

To be able to determine the variation tread of a single factor and to determine the superior leaching conditions of a single factor, we designed experiments as follows. The extraction experiments were performed in a 500-mL spherical glass reactor equipped with a mechanical stirrer and a temperature control unit. First, the experiment was designed for a set of basic conditions. The reactor was filled with 5 g of dross and 40 mL of 0.8 $mol \cdot L^{-1}$ NaOH solution. The experiment was conducted at 313 K with a stirring speed of 100 $r \cdot min^{-1}$. A series of single factor experiments were then conducted by varying the process parameters as follows: extraction temperature (313–353 K), concentration of the NaOH solution (0.4–2.4 $mol \cdot L^{-1}$), stirring speed (50–300 $r \cdot min^{-1}$), and liquid-to-solid ratio, i.e., the ratio of the NaOH solution to the dross (4 to 24 $mL \cdot g^{-1}$). To study the extraction kinetics of the soluble aluminum from the dross, the following experimental conditions were employed: 40 mL NaOH solution of 1.0 $mol \cdot L^{-1}$, 5 g of dross, stirring speed of 100 $r \cdot min^{-1}$, and reaction temperature in the range 308–348 K. In each experiment, the solution was sampled at intervals of 2 min for the duration 1–15 min. Similarly, to study the kinetics of AlN hydrolysis from the dross, the reaction temperature was varied in the range 313–353 K and the solution was sampled in each experiment at intervals of 5 min for the duration 5–30 min.

The experimental procedure was as follows. The NaOH solution was added to the reactor with dross, where the latter was bathed at a constant temperature, and $NH_3$ gas from the extraction system was absorbed with $H_2SO_4$ solution. After extraction, the solution and the extracted slag were separated rapidly. The remaining $NH_3$ in the solution was distilled along with the $H_2SO_4$ solution for analysis.

The extracted slag was dried at 60°C for 48 h and then mixed with MgO in a blender mixer. The composition of the mixture was 87.34wt% dried slag and 12.66wt% MgO. The mixture was molded into a cylinder with 3wt% polyvinyl alcohol under a pressure of 25 MPa and then pressed into discs, each 1 cm thick and 2.5 cm in diameter. An aluminum crucible with a disc was placed inside the hot zone of an electric furnace for calcination in the range 1373–1773 K for 3 h in air. Both sides of the corundum furnace were sealed with a quartz plug. The temperature of the furnace was cooled from calcination temperature to 773 K with the decreasing speed of 4–5°C·$min^{-1}$. The samples were then cooled to room temperature for analysis. The technical route of the experiment is shown in Fig. 2.

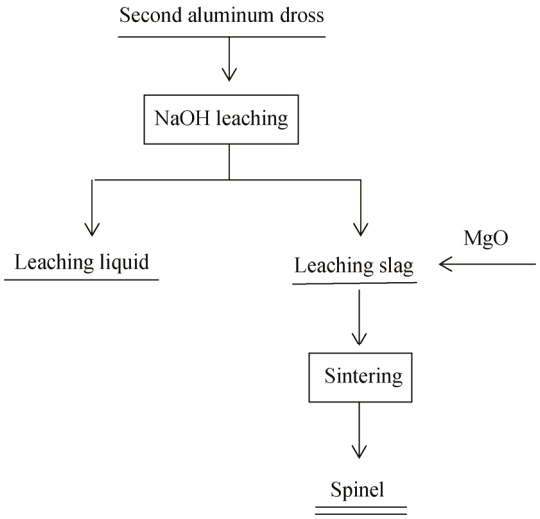


**Fig. 2. Technical route of the experiment.**

### 2.3. Sample analysis

The microstructure of the sample powders was determined using scanning electron microscopy (SEM, JSM-6360 V, Japan) [18]. The mineral phases of the samples were analyzed by X-ray diffraction (XRD, D/MAX 2500X, Japan) with Cu $K_\alpha$ as the radiation source operated at 40 mA and 200 kV [19–22]. The elemental composition of the dross was examined by X-ray fluorescence (XRF-AXIOS, PANalytical, Netherlands), and the particle size distribution was analyzed by laser particle analysis (OMEC LS-POP, China). The concentration of water-soluble aluminum was determined according to the Chemical reagent–General method for the determination of aluminum (GB/T 9734—2008). The concentration of ammonia nitrogen in solution was determined according to the method for the determination of ammonia nitrogen in water quality-salicylic acid spectrophotometry (HJ 536-2009). The powders were pressed using a hydraulic press (YLJ-40T, China), and the compression strength was tested using an electrohydraulic-type compression machine (TYA-100C, China).

### 2.4. Data analysis

The extraction percentage of total aluminum, $x_1$, and the hydrolysis percentage of AlN, $x_2$, from the dross were calculated as

$$x_1 = \frac{VC_1M_1}{m\omega_1} \times 100\% \quad (1)$$

$$x_2 = \frac{VC_2M_2}{m\omega_2} \times 100\% \quad (2)$$

where $m$ is the mass of the dross, g; $\omega_1$ and $\omega_2$ are the contents (mass fraction) of total aluminum and total AlN in the dross, respectively; $V$ is the volume of the extracting solution, L; $C_1$ is the concentration of soluble $Al^{3+}$ in solution and $C_2$ is the part of hydrolyzed aluminum from AlN, $mol \cdot L^{-1}$; and $M_1$ and $M_2$ are the atomic mass and molecular mass of Al and AlN ($g \cdot mol^{-1}$), respectively. The extraction percentage of soluble aluminum, $x_3$, was calculated as follows:

$$x_3 = \frac{m_3 - m_2}{m_3} \times 100\% \quad (3)$$

where $m_2$ is the mass of soluble AlN, and $m_3$ is the mass of soluble aluminum.

The extraction percentage was fitted with the equation [23]:

$$1 - (1 - x_i)^{\frac{2}{3}} = kt \quad (4)$$

where $x_i$ ($i$ = 1, 2, and 3), $k$, and $t$ are the extraction percentage, reaction constant, and extraction time (min), respectively.

The activation energy was calculated according to the Arrhenius equation [24]:

$$\ln k = \ln A - \frac{E}{RT} \quad (5)$$

where $k$ is the reaction rate constant, $A$ is the pre-exponential factor, $E$ is the reaction energy, $R$ is the mole gas constant, and $T$ is the thermodynamic temperature.

## 3. Results and discussion

### 3.1. Extraction of soluble aluminum and hydrolysis of AlN from secondary aluminum dross

Fig. 3 shows the effect of the extraction conditions on the extraction percentage of the soluble aluminum and the hydrolysis percentage of AlN from the dross. As the temperature increased from 303 to 353 K, the extraction percentage of the soluble aluminum increased from 31.55% to 74.80% and the hydrolysis percentage of AlN increased from 10.71% to 40.71% (Fig. 3(a)). The increase in temperature reduced the surface boundary layer of the dross particles [25], thereby decreasing the resistance of soluble aluminum from the dross to the NaOH solution. This effect also improved the diffusion coefficient with increasing temperature. The results show that temperature more strongly influenced the extraction of the soluble aluminum than the AlN hydrolysis. The two parameters were also strongly affected by the concentration of the NaOH solution (Fig. 3(b)). The extraction percentage of soluble aluminum increased from 20.05% to 78.70%, whereas the hydrolysis percentage of AlN increased from 12.59% to 52.09% when the NaOH concentration was increased from 0.4 to 2.4 $mol \cdot L^{-1}$. The extraction percentage of soluble aluminum and the hydrolysis percentage of AlN are not significant improved when the NaOH

concentration was higher than 1.6 mol·L$^{-1}$. These effects could be due to the transformation of $Al^{3+}$ to the $Al(OH)_4^-$ species at high NaOH concentrations [24]. Fig. 3(c) shows that the extraction percentage of soluble aluminum and the hydrolysis percentage of AlN from the dross increased with increasing stirring speed; faster stirring promoted mass transfer in the dross–solution system and enhanced the reaction in solution. Likewise, the extraction percentage of the soluble aluminum improved substantially to 82.60% as the liquid-to-solid ratio was increased to 12 mL·g$^{-1}$, which is attributed to the concentration of potential. The concentration of potential increased as the liquid-to-solid ratio improved. The liquid-to-solid ratio, however, had a lesser impact on the hydrolysis percentage of AlN, which increased from 13.79% to 29.29% (Fig. 3(d)). On the basis of the aforementioned results, the optimal extraction performance of soluble aluminum and hydrolyzed aluminum from AlN were obtained under the following conditions: a temperature of 353 K, NaOH concentration of 1.6 mol·L$^{-1}$, liquid-to-solid ratio (NaOH to dross) of 12 mL·g$^{-1}$, stirring speed of 300 r·min$^{-1}$, and an extraction period of 15 min for soluble aluminum and a hydrolysis period of 30 min for AlN. Under these conditions, the extraction percentage of soluble aluminum from secondary aluminum dross was as high as 80% and the hydrolysis percentage of AlN reached 40%.

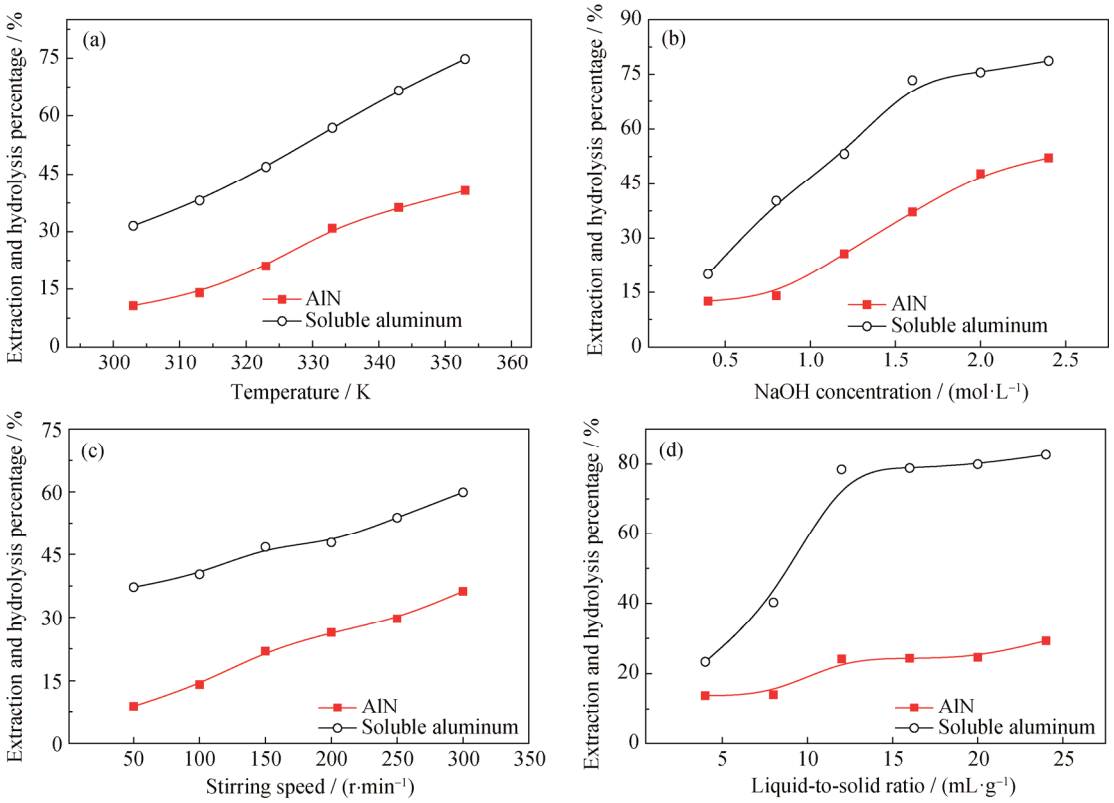


**Fig. 3. Effect of temperature (a), NaOH concentration (b), stirring speed (c), and liquid-to-solid ratio (d) on the extraction of soluble aluminum and on AlN hydrolysis from the dross.**

### 3.2. Kinetics of soluble aluminum extraction and AlN hydrolysis from secondary aluminum dross

The kinetic parameters of soluble aluminum extraction and AlN hydrolysis were calculated according to the Arrhenius equation. The extraction temperature clearly influenced the extraction percentage of soluble aluminum but affected the AlN hydrolysis percentage to a lesser extent (Fig. 4). As the temperature was increased from 308 to 348 K, the extraction percentage of soluble aluminum improved from 61.65% to 79.71% after 15 min and most of the extraction occurred within 5 min. However, as the temperature was increased from 313 to 353 K, the hydrolysis percentage of AlN improved from 18.14% to only 37.20% after 30 min.

The results of the analysis, including the correlation coefficient for the fit with the outer diffusion model without a product layer are shown in Table 2. The Arrhenius plot was obtained using the apparent rate constant (Fig. 5). The activation energies of soluble aluminum extraction and AlN hydrolysis were 7.15 kJ·mol$^{-1}$ and 8.98 kJ·mol$^{-1}$, respectively.

The activation energy of controlled-rate outer diffusion is typically in the range from 4 to 12 kJ·mol$^{-1}$ [24]. These results suggest that the NaOH solution-based extraction of soluble aluminum and the hydrolysis of AlN from the dross were kinetically controlled by outer diffusion without a product layer.

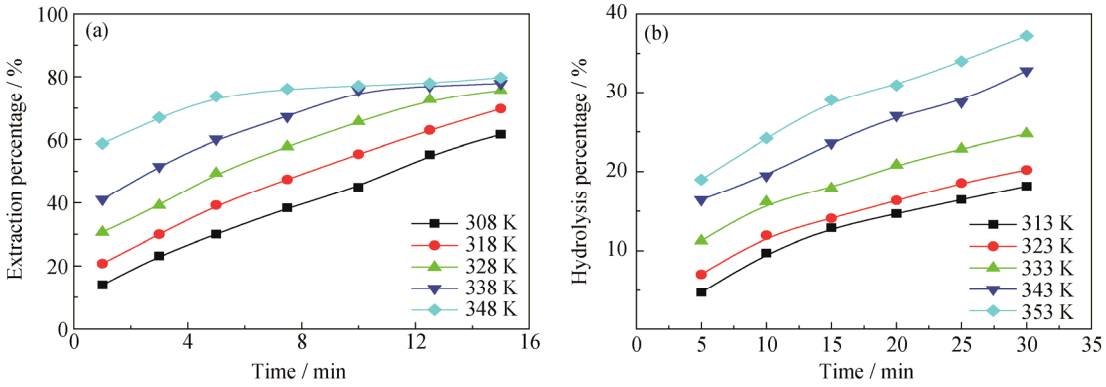


**Fig. 4. Effect of temperature on the extraction percentage of soluble aluminum (a) and the hydrolysis percentage of AlN from the dross (b).**

**Table 2. Apparent rate constants and correlation coefficients**

| Substance | $T$ / K | Linear regression equation | Apparent rate constant, $k$ / min$^{-1}$ | ln($k$ / min$^{-1}$) | Coefficient, $R^2$ |
|---|---|---|---|---|---|
| Soluble aluminum | 308 | $1-(1-x)^{2/3}=0.0266t+0.0752$ | 0.0266 | –3.63 | 0.997 |
| | 318 | $1-(1-x)^{2/3}=0.0287t+0.127$ | 0.0287 | –3.55 | 0.997 |
| | 328 | $1-(1-x)^{2/3}=0.0316t+0.193$ | 0.0316 | –3.45 | 0.995 |
| | 338 | $1-(1-x)^{2/3}=0.0340t+0.275$ | 0.0340 | –3.38 | 0.993 |
| | 348 | $1-(1-x)^{2/3}=0.0340t+0.41148$ | 0.0340 | –3.33 | 0.999 |
| AlN | 313 | $1-(1-x)^{2/3}=0.00354t+0.0254$ | 0.00354 | –5.64 | 0.947 |
| | 323 | $1-(1-x)^{2/3}=0.00386t+0.0333$ | 0.00386 | –5.56 | 0.990 |
| | 333 | $1-(1-x)^{2/3}=0.00415t+0.0597$ | 0.00415 | –5.48 | 0.993 |
| | 343 | $1-(1-x)^{2/3}=0.00474t+0.0899$ | 0.00474 | –5.35 | 0.989 |
| | 353 | $1-(1-x)^{2/3}=0.00521t+0.114$ | 0.00521 | –5.26 | 0.978 |

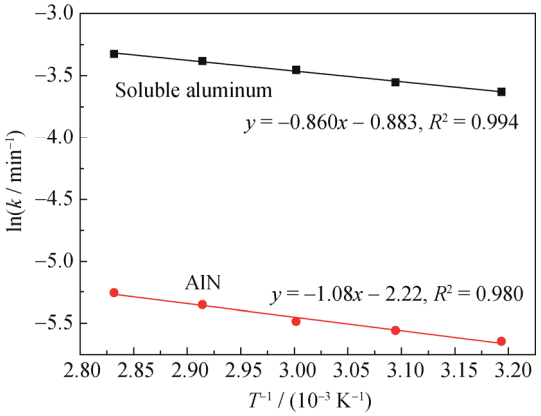


**Fig. 5. Relationship between ln$k$ and $T^{-1}$.**

### 3.3. Mechanism of soluble aluminum extraction from secondary aluminum dross

The use of NaOH improved the extraction percentage of soluble aluminum from the dross. Intermediate species such as $[Al(OH)]^{2+}$, $[Al(OH)_2]^{+}$, and $Al(OH)_3$ tended to form prior to the generation of the final product, $[Al(OH)_4]^{-}$. The reactions may proceed as follows [26–28]:

$$Al^{3+} + OH^- \rightarrow [Al(OH)]^{2+} \quad (6)$$

$$[Al(OH)]^{2+} + OH^- \rightarrow [Al(OH)_2]^{+} \quad (7)$$

$$[Al(OH)_2]^{+} + OH^- \rightarrow Al(OH)_3 \quad (8)$$

$$Al(OH)_3 + OH^- \rightarrow [Al(OH)_4]^{-} \quad (9)$$

Fig. 6 shows that the dross particles had a rough, angular, irregular, and porous microstructure. Some parts seemed spherical; however, the particles exhibited a smooth surface after extraction. The yellow in Fig. 6 represents elemental aluminum. Before extraction, elemental aluminum was observed mainly on the particles; after extraction, the yellow became darker, indicating that some parts of the soluble aluminum had dissolved.

### 3.4. Synthesis of $MgAl_2O_4$ spinel from the extracted slag

Fig. 7 reveals that the main phases in the extracted slag

were $MgAl_2O_4$ and corundum at the conditions of a temperature of 353 K, NaOH concentration of 1.6 mol·L$^{-1}$, liquid-to-solid ratio of 12 mL·g$^{-1}$, stirring speed of 300 r·min$^{-1}$, and a period of 30 min. The $MgAl_2O_4$ was present in the form of crystal seeds, which enhanced the synthesis of $MgAl_2O_4$ spinel and formed heterogeneous nucleation substrates. According to heterogeneous nucleation theory [29], $MgAl_2O_4$ crystal seeds can decrease the potential barrier for nucleation and, hence, accelerate the nucleation and growth of $MgAl_2O_4$ spinel.

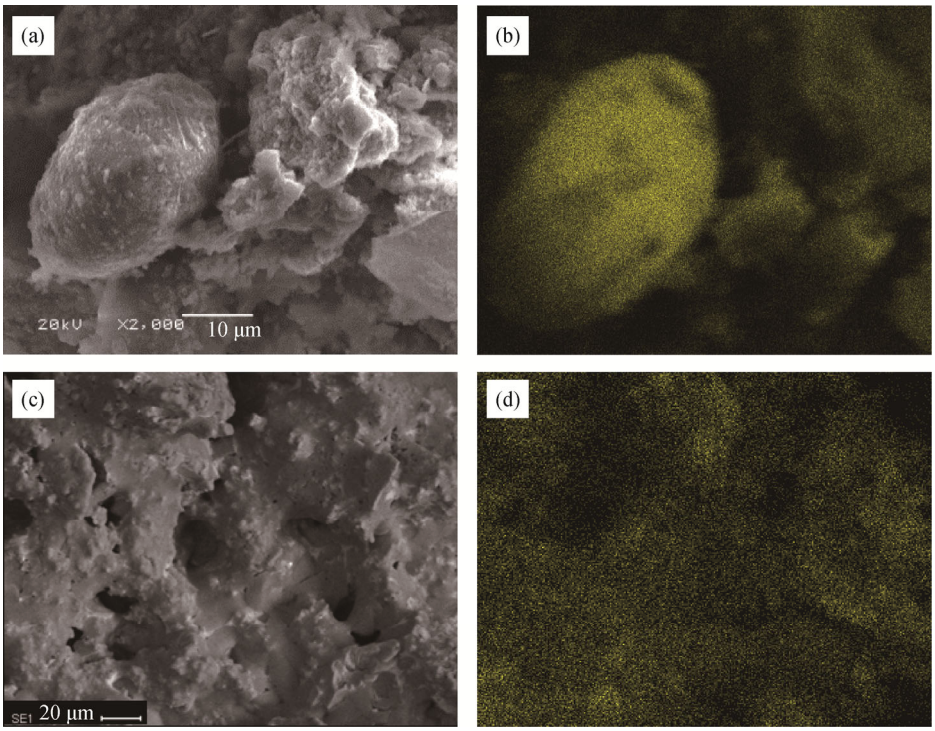


**Fig. 6. SEM images and elemental Al mapping analysis of the dross (a, b) before and (c, d) after extraction with NaOH.**

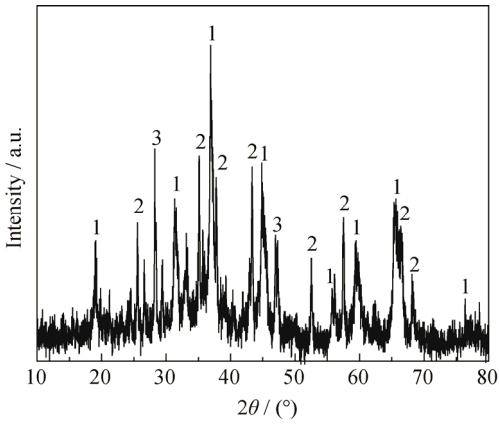


**Fig. 7. XRD pattern of the extracted slag. 1—$MgAl_2O_4$; 2—α-$Al_2O_3$; 3—$CaF_2$.**

The rate of nucleation in a unit area of the substrate can be expressed as

$$I^{\mathrm{h}} = K^{\mathrm{h}} \exp\left(-\frac{\Delta G_{\mathrm{k}}^{\mathrm{h}}}{RT}\right) \tag{10}$$

where $I^{\mathrm{h}}$ is the rate of nucleation in a unit area of the substrate, $K^{\mathrm{h}}$ is a constant independent of the substrate, $R$ is the universal gas constant, $T$ is the temperature, and $\Delta G_{\mathrm{k}}^{\mathrm{h}}$ is the potential barrier for heterogeneous nucleation and can be expressed as

$$\Delta G_{\mathrm{k}}^{\mathrm{h}} = \Delta G_{\mathrm{k}} \frac{1}{4}\left((2+\cos\theta)(1-\cos\theta)^2\right) \tag{11}$$

where $\Delta G_{\mathrm{k}}$ is the potential barrier for homogeneous nucleation and $\theta$ is the contact angle between the crystal nuclei and the substrate. When the substrate is identical to the nucleating crystal, $\theta = 0°$ and, consequently, $\Delta G_{\mathrm{k}}^{\mathrm{h}} = 0$; i.e., there is no potential barrier to nucleation. However, when significant differences exist between the substrate and the nucleating crystal, i.e., $\theta = 180°$ and, hence, $\Delta G_{\mathrm{k}}^{\mathrm{h}} = \Delta G_{\mathrm{k}}$, they cannot interact; therefore, nucleation cannot be accelerated. On the basis of this theory, we can infer that the $MgAl_2O_4$ crystal seeds could decrease the potential barrier for nucleation and thereby accelerate the nucleation and growth of $MgAl_2O_4$.

According to the basic principles of thermodynamics, along with the thermodynamic data of the compounds $Al_2O_3$, MgO, and $MgAl_2O_4$ at 298 K, the reaction between MgO and $Al_2O_3$ proceeds as follows:

$$MgO+Al_2O_3 = MgAl_2O_4,$$
$$\Delta G^{\ominus} = -35600 - 2.09T \text{ , J·mol}^{-1} \quad (12)$$

Fig. 8 shows that the Gibbs free energy of the reaction was negative when the sintering temperature was in the range 1373–1773 K, and the generation of $MgAl_2O_4$ occurred spontaneously under standard conditions. Thus, the extracted slag containing MgO is deemed viable for use in the production of $MgAl_2O_4$ spinel.

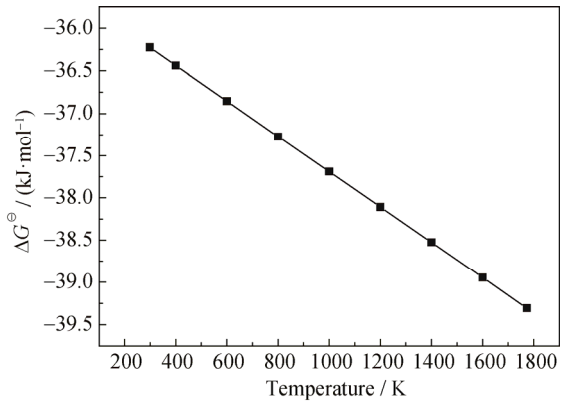


**Fig. 8. Relationship between Gibbs free energy and temperature according to Eq. (12).**

According to the XRD patterns (Fig. 9), $MgAl_2O_4$ was formed when the samples were sintered at 1373, 1473, 1573, 1673, and 1773 K. The diffraction peaks of the $MgAl_2O_4$ spinel sintered at 1673 K were stronger than that of the samples sintered at other temperatures, and compounds such as corundum, $(Na,Ca)Al(Si,Al)_3O_8$, and $(Ca,Na)(Si,Al)_4O_8$ were not formed at 1673 K, suggesting that this was an optimal sintering temperature. The content of $MgAl_2O_4$ spinel was greater than 70wt% at the sintering temperature of 1673 K. The secondary aluminum dross after extraction could be used as a raw material to obtain $MgAl_2O_4$ spinel.

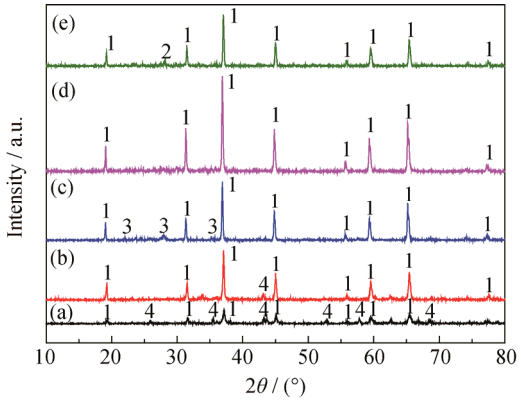


**Fig. 9. XRD patterns of $MgAl_2O_4$ from extracted slag after sintering at different temperatures: (a) 1373 K; (b) 1473 K; (c) 1573 K; (d) 1673 K; (e) 1773 K. 1—$MgAl_2O_4$; 2—$(Ca,Na)(Si,Al)_4O_8$; 3—$(Na, Ca)Al(Si, Al)_3O_8$; 4—$Al_2O_3$.**

The results of the XRD analysis were further confirmed by the results of the Fourier transform infrared spectroscopy (FT-IR) analysis. Fig. 10 shows the FT-IR spectra of the $MgAl_2O_4$ powders sintered from secondary aluminum dross at 1473–1773 K. Two small and broad peaks appeared at about 690 and 530 cm$^{-1}$, indicating the formation of the $MgAl_2O_4$ spinel. The strong, broad bands at about 3400 and 1600 cm$^{-1}$ established the presence of molecular water in the structure [30–31]. The higher-frequency band is associated with the O–H stretching vibrations (symmetric and antisymmetric) of molecular water, whereas the low frequency is due to the H–O–H bending mode [32]. The results of the FT-IR analysis are in accordance with the XRD data. The product sintered from secondary aluminum dross was primarily $MgAl_2O_4$.

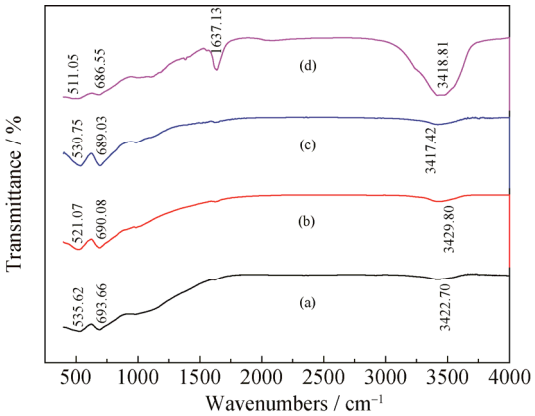


**Fig. 10. FT-IR spectra of $MgAl_2O_4$ from extracted slag sintered at different temperatures: (a) 1473 K; (b) 1573 K; (c) 1673 K; (d) 1773 K.**

The Raman peaks for the $MgAl_2O_4$ spinel can be determined from group theory. Natural $MgAl_2O_4$ spinel is assumed to have a close-packed, face-centered-cubic structure described by the *Fd*3*m* space group, with eight molecular units per cubic cell. The correlation between the site and crystal symmetries enables the identification of the irreducible representations that describe the normal modes of vibration associated with each atomic species at the center of the Brillouin zone [33–34]. Table 3 shows the Raman spectra of the $MgAl_2O_4$ spinel powders sintered from secondary aluminum dross at 1473–1773 K. The peaks near 406 cm$^{-1}$ are attributed to the $AlO_4$ bending. The shoulder peak on the low-wavenumber side of the 406 cm$^{-1}$ peak corresponds to the additional bending vibrations of the Al ions in the tetrahedral sites. The peaks near 723 cm$^{-1}$ are associated with the stretching of the $AlO_4$ tetrahedra. The peaks near 766 cm$^{-1}$ correspond to the Mg–O stretching vibrations, and these peaks become increasingly sharp with increasing sintering temperature. Furthermore, the peaks near 723 cm$^{-1}$ decrease in intensity at higher sintering temperatures (1673–1773 K), indi-

cating more order for the spinel at higher temperatures [33–34], which is also in accordance with the XRD results.

Fig. 11 shows that the microstructure of the powders was more compact and homogeneous in the sample sintered at 1673 K than those in the samples sintered at 1473, 1573, and 1773 K. This result is likely due to exaggerated grain growth at 1773 K. The co-existence of metal oxide (e.g., CaO) and nonmetal components (e.g., $SiO_2$) in the extracted slag may have led to the formation of the liquid glassy phase. The viscosity of this phase was reduced by the formation of weak Si–O bonds, which altered the melting characteristics of the spinel during sintering [35].

**Table 3. Raman peaks in $MgAl_2O_4$ spinel powders sintered at different temperatures**

| Sintering temperature / K | Peak position / $cm^{-1}$ | | | | |
|---|---|---|---|---|---|
| | $F_{2g}$ 306.90* | $E_g$ 406.00* | $F_{2g}$ 670.00* | $A_{1g}$ 723.00* | $A_{1g}$ 766.00* |
| 1473 | 309.47 | 407.94 | 663.39 | 725.05 | 764.69 |
| 1573 | 313.28 | 413.58 | 663.39 | 723.25 | 764.69 |
| 1673 | 305.71 | 402.34 | 661.62 | 719.68 | 762.94 |
| 1773 | 307.62 | 409.87 | 668.90 | 721.49 | 768.33 |

Note: $F_{2g}$, $E_g$, and $A_{1g}$ represent the peak positions, $cm^{-1}$; * Data of reference.

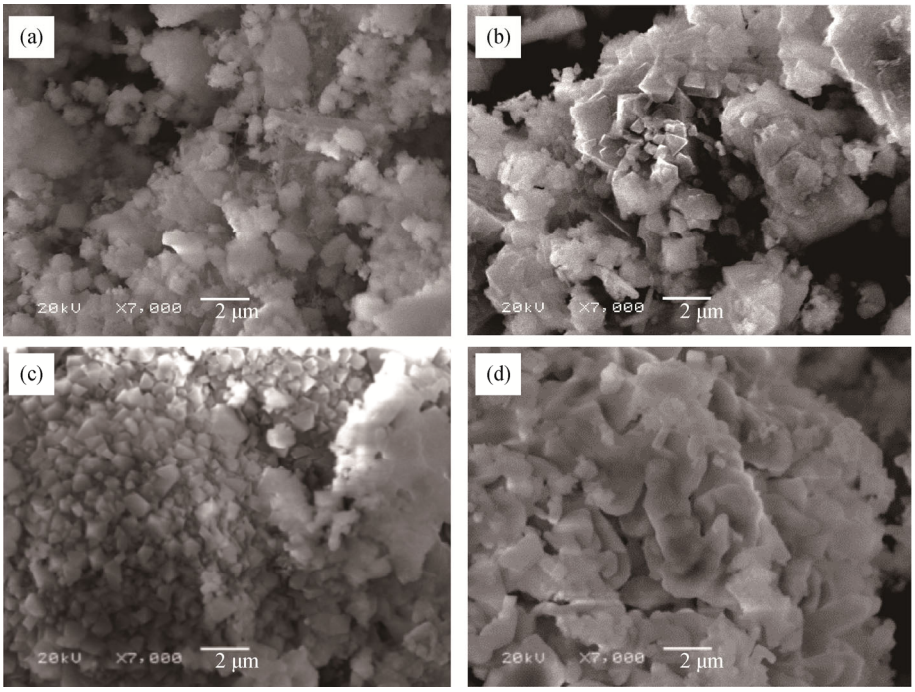


**Fig. 11. SEM images of $MgAl_2O_4$ powders obtained from extracted slag sintered at different temperatures: (a) 1473 K; (b) 1573 K; (c) 1673 K; (d) 1773 K.**

Table 4 lists the compressive strength of the samples sintered at different temperatures for 3 h. From Table 4, it can be found that the compressive strength of the spinel increased substantially with increasing sintering temperature, rising from 50.8 to 64.3 MPa as the temperature was increased from 1473 to 1573 K. An increase in temperature from 1673 to 1773 K resulted in a slight increase in compressive strength from 69.4 to 70.2 MPa. Nevertheless, these values are greater than the threshold (40 MPa), prescribed by the National Standard for Magnesia and Magnesia–alumina Refractory Bricks of China (GB/T 2275—2007). The compressive strength of the product obtained at 1773 K was higher than that of the product obtained at 1673 K; however, the difference was slight, suggesting that a sintering temperature of 1673 K was optimal.

**Table 4. Compressive strength of the samples sintered at different temperatures for 3 h**

| Temperature / K | 1473 | 1573 | 1673 | 1773 | GB / T 2275—2007 |
|---|---|---|---|---|---|
| Compressive strength / MPa | 50.80 | 64.30 | 69.40 | 70.20 | 40 |

## 4. Conclusions

(1) The optimized conditions for extraction of soluble aluminum and for hydrolysis of AlN from secondary aluminum dross were as follows: a temperature of 353 K, a liquid-to-solid ratio (of 1.6 $mol \cdot L^{-1}$ NaOH to dross) of 12 $mL \cdot g^{-1}$, a stirring speed of 300 $r \cdot min^{-1}$, and a process duration of 15 min for soluble aluminum extraction and 30 min

for AlN hydrolysis. Under these conditions, the percentage of soluble aluminum extraction and AlN hydrolysis from the dross reached 80% and 40%, respectively. The extraction and hydrolysis were controlled by outer diffusion without a product layer, and the activation energies of the two reactions were 7.15 and 8.98 $kJ \cdot mol^{-1}$, respectively.

(2) The slag extracted contained $MgAl_2O_4$ and corundum and could be sintered to produce $MgAl_2O_4$ spinel. The compressive strength of the $MgAl_2O_4$ spinel was as high as 69.4 MPa when the slag was sintered at 1673 K for 3 h. This value exceeds the threshold (40 MPa) prescribed in the National Standard for the Magnesia and Magnesia–alumina Refractory Bricks of China (GB/T 2275–2007).

## Acknowledgements

This work was financially supported by the National Natural Science Foundation of China (No. 21577176) and the Environment Protection Scientific Research Project of Hunan Province, China (No. [2016]59-3).

## References

[1] J.P. Hong, J. Wang, H.Y. Chen, B.D. Sun, J.J. Li, and C. Chen, Process of aluminum dross recycling and life cycle assessment for Al–Si alloys and brown fused alumina, *Trans. Nonferrous Met. Soc. China*, 20(2010), No. 11, p. 2155.

[2] A. López-Delgado, H. Tayibi, C. Pérez, F.J. Alguacil, and F.A. López, A hazardous waste from secondary aluminium metallurgy as a new raw material for calcium aluminate glasses, *J. Hazard. Mater.*, 165(2009), No. 1-3, p. 180.

[3] J.A.S. Tenorio and D.C.R. Espinosa, Effect of salt/oxide interaction on the process of aluminum recycling, *J. Light Met.*, 2(2002), No. 2, p. 89.

[4] P.E. Tsakiridis, Aluminum salt slag characterization and utilization-A review, *J. Hazard. Mater.*, 217-218(2012), p. 3.

[5] M.C. Shinzato and R. Hypolito, Solid waste from aluminum recycling process: characterization and reuse of its economically valuable constituents, *Waste Manage.*, 25(2005), No. 1, p. 37.

[6] P.E. Tsakiridis, P. Oustadakis, and S. Agatzini-Leonardou, Aluminum recovery during black dross hydrothermal treatment, *J. Environ. Chem. Eng.*, 1(2013), No. 1-2, p. 23.

[7] G.V. Calder and T.D. Stark, Aluminum reactions and problems in municipal solid waste landfills, *Pract. Period. Hazard. Toxic Radioact. Waste Manage.*, 14(2010), No. 4, p. 258.

[8] J.Y. Hwang, X. Huang, and Z. Xu, Recovery of metals from aluminum dross and salt cake, *J. Miner. Mater. Charact. Eng.*, 5(2006), No. 1, p. 47.

[9] B. Dash, B.R. Das, B.C. Tripathy, I.N. Bhattacharya, and S.C. Das, Acid dissolution of alumina from waste aluminum dross, *Hydrometallurgy*, 92(2008), No. 1-2, p. 52.

[10] M. Davies, P. Smith, W.J. Bruckard, and J.T. Woodcock, Treatment of salt cakes by aqueous leaching and Bayer-type digestion, *Miner. Eng.*, 21(2008), No. 8, p. 605.

[11] K. Taehyung, K. Donghyun, and K. Shinhoo, Effect of additives on the sintering of $MgAl_2O_4$, *J. Alloys Compd.*, 587(2014), p. 594.

[12] H.N. Yoshimura, A.P. Abreu, A.L. Molisani, A.C. de Camargo, J.C.S. Portela, and N.E. Narita, Evaluation of aluminum dross waste as raw material for refractories, *Ceram. Int.*, 34(2008), No. 3, p. 581.

[13] F. Tavangarian and R. Emadi, Synthesis and characterization of pure nanocrystalline magnesium aluminate spinel powder, *J. Alloys Compd.*, 489(2010), No. 2, p. 600.

[14] I. Ganesh, G.J. Reddy, G. Sundararajan, S.M. Olhero, P.M.C. Torres, and J.M.F. Ferreira, Influence of processing route on microstructure and mechanical properties of $MgAl_2O_4$ spinel, *Ceram. Int.*, 36(2010), No. 2, p. 473.

[15] Z.Y. Yu, N.Q. Zhao, E.Z. Liu, C.S. Shi, X.W. Du, and J. Wang, Fabrication of aluminum matrix composites with enhanced mechanical properties reinforced by in situ generated $MgAl_2O_4$ whiskers, *Composites Part A*, 43(2012), No. 4, p. 631.

[16] I. Ganesh, Fabrication of magnesium aluminate ($MgAl_2O_4$) spinel foams, *Ceram. Int.*, 37(2011), No. 7, p. 2237.

[17] G. Bonnefont, G. Fantozzi, S. Trombert, and L. Bonneau, Fine-grained transparent $MgAl_2O_4$ spinel obtained by spark plasma sintering of commercially available nanopowders, *Ceram. Int.*, 38(2012), No. 1, p. 131.

[18] F. Zhu, J.X. Liao, S.G. Xue, W. Hartley, Q. Zhou, and H. Wu, Evaluation of aggregate microstructures following natural regeneration in bauxite residue as characterized by synchrotron-based X-ray micro-computed tomography, *Sci. Total Environ.*, 573(2016), p. 157.

[19] M. Li, B. Peng, L.Y. Chai, N. Peng, H. Yan, and D.K. Hou, Recovery of iron from zinc leaching residue by selective reduction roasting with carbon, *J. Hazard. Mater.*, 237-238(2012), p. 323.

[20] Y. Zhang, Z.H. Guo, Z.Y. Han, and X.Y. Xiao, Effect of rare earth oxides doping on $MgAl_2O_4$ spinel obtained by sintering of secondary aluminium dross, *J. Alloys Compd.*, 735(2018), p. 2597.

[21] Z.Y. Han, Z.H. Guo, Y. Zhang, X.Y. Xiao, Z. Xu, and Y. Sun, Adsorption-pyrolysis technology for recovering heavy metals in solution using contaminated biomass phytoremediation, *Resour. Conserv. Recycl.*, 129(2018), p. 20.

[22] X.F. Kong, M. Li, S.G. Xue, W. Hartley, C.R. Chen, C. Wu, X.F. Li, and Y.W. Li, Acid transformation of bauxite residue: Conversion of its alkaline characteristics, *J. Hazard. Mater.*, 324(2017), Part B, p. 382.

[23] H.G. Li, *Metallurgical Principle*, Science Press, Beijing, 2005, p. 300.

[24] R.C. Wang, Y.C. Zhai, Z.Q. Ning, and P.H. Ma, Kinetics of $SiO_2$ leaching from $Al_2O_3$ extracted slag of fly ash sodium hydroxide solution, *Trans. Nonferrous Met. Soc. China*, 24(2014), No. 6, p. 1928.

[25] H.D. Chandler, Activation entropy and anomalous tempera-

ture dependence of viscosity in aqueous suspensions of $Fe_2O_3$, *Powder Technol.*, 305(2017), p. 572.

[26] X.B. Li, W.J. Lv, G.T. Feng, G.H. Liu, Z.H. Peng, Q.S. Zhou, and Y. Meng, The applicability of Debye-Hückel model in $NaAl(OH)_4$–NaOH–$H_2O$ system, *Chin. J. Process Eng.*, 5(2005), No. 5, p. 525.

[27] S. Wang, *Preparation and Properties of Spinel Composites From Secondary Aluminium Dross* [Dissertation], Central South University, Changsha, 2016, p. 6.

[28] X.F. Kong, Y. Guo, S.G. Xue, W. Hartley, C. Wu, Y.Z. Ye, and Q.Y. Cheng, Natural evolution of alkaline characteristics in bauxite residue, *J. Cleaner Prod.*, 143(2017), p. 224.

[29] X.L. Jia, H.J. Zhang, Y.J. Yan, and Z.J. Liu, Effect of the citrate sol–gel synthesis on the formation of $MgAl_2O_4$ ultrafine powder, *Mater. Sci. Eng. A*, 379(2004), No. 1-2, p. 112.

[30] H.B. Bafrooei and T. Ebadzadeh, $MgAl_2O_4$ nanopowder synthesis by microwave assisted high energy ball-milling, *Ceram. Int.*, 39(2013), No. 8, p. 8933.

[31] J.J. Guo, H. Lou, H. Zhao, X.G. Wang, and X.M. Zheng, Novel synthesis of high surface area $MgAl_2O_4$ spinel as catalyst support, *Mater. Lett.*, 58(2004), No. 12-13, p. 1920.

[32] M.F. Zawrah, H. Hamaad, and S. Meky, Synthesis and characterization of nano $MgAl_2O_4$ spinel by co-precipitated method, *Ceram. Int.*, 33(2007), No. 6, p. 969.

[33] N. Van Minh and I.S. Yang, A Raman study of cation disorder transition temperature of natural $MgAl_2O_4$ spinel, *Vib. Spectrosc.*, 35(2004), No. 1-2, p. 93.

[34] P. Barpanda, S.K. Behera, P.K. Gupta, S.K. Pratihar, and S. Bhattacharya, Chemically induced order disorder transition in magnesium aluminum spinel, *J. Eur. Ceram. Soc.*, 26(2006), No. 13, p. 2603.

[35] M.L. Bouchetou, J.P. Ildefonse, J. Poirier, and P. Daniellou, Mullite grown from fired andalusite grains: the role of impurities and of the high temperature liquid phase on the kinetics of mullitization and consequences on thermal shocks resistance, *Ceram. Int.*, 31(2005), No. 7, p. 999.